JOURNAL OF AIRCRAFT
Vol. 47, No. 5, September–October 2010

Engineering Notes

Coaxial Rotor Helicopter in Hover Based on Unstructured Dynamic Overset Grids

He-yong Xu* and Zheng-yin Ye†
Northwestern Polytechnical University, 710072 Xi'an, People's Republic of China

DOI: 10.2514/1.C031079

I. Introduction

COAXIAL rotor configuration is one of the technological solutions for increasing helicopter forward speed, maneuverability, and load-carrying ability. Since two rotors produce the net thrust instead of a single rotor in the conventional design, the diameter of the rotors can be reduced to carry the same amount of weight. The most attractive feature of a coaxial design is the resulting compactness and safety of the vehicle. Second, the antitorsional moment generated by the two rotors would be canceled due to the opposite rotational directions, and the tail rotor and tail boom can be eliminated, resulting in a smaller and lighter vehicle.

Compared to the individual-rotor helicopter, the aerodynamics and flow physics of coaxial rotor helicopter are relatively less studied and understood. The method of slipstream theory was first used to study the coaxial rotor, and then the predicted wake vortex model [1,2], free wake vortex model [3], and vorticity transport model [4,5] were applied to the coaxial rotor analysis. All the methods above carry out some approximations to the rotor, and the detailed flow feature near the blades and blade vortex in the wake cannot be simulated. Recently, the unsteady Navier–Stokes equations were used to simulate the coaxial rotor flows [6–8] to provide a detailed understanding of the flow physics of coaxial rotor.

In the present Note, the three-dimensional unsteady Euler equations were solved to simulate the unsteady flows around coaxial rotor helicopter and individual-rotor helicopter in hover based on the unstructured dynamic overset grids. The aerodynamic interaction property of the coaxial rotor helicopter in hover and the effect of fuselage on the unsteady performance were studied.

II. Calculating Model and Overset Grids Generation

For the lack of a standard model of a coaxial rotor helicopter, we use an assembled model here. The fuselage model of the NASA ROBIN (rotor-body interaction) configuration is used for the coaxial rotor helicopter's fuselage, and the coaxial rotor is a two-layer four-blade rotor.

The two-layer rotors rotate at an opposite direction with a high velocity when the coaxial rotor is in working condition. For the effective treatment of the complicated flowfield involving the relative motion between the blades and the fuselage, the computational domain is decomposed into three subzones. The two rotational subzones contain the top and bottom rotors, respectively, and rotate with them. The stationary subzone covers the remainder of the flowfield, including the fuselage and the far wake of the rotor.

After grid generation, we can obtain the unstructured overset grids for the coaxial rotor helicopter configuration, containing three subzone meshes, as shown in Fig. 1. The slice meshes of the top rotor subzone and bottom subzone and fuselage subzone are shown in Figs. 1a–1c, respectively, and the overlapping drawing of the slice meshes is shown in Fig. 1d. The numbers of grid elements of the three subzones are 737,790, 737,488, and 810,968, respectively. The procedure of generating unstructured overset grid is given in detail in [9]. This method can ensure that there is always a reasonable overlapping area between overset subzones at every time stepping during the unsteady simulation, without any hole boundary regeneration and inverse map grid generation, which increases the efficient of overset-grid generation and unsteady simulation.

III. Numerical Method

A. Governing Equations

The unsteady Euler equations in an arbitrary Lagrangian–Eulerian formulation [10] are discretized by a center finite volume method on the inertial coordinate system. The integral form of unsteady Euler equations for a bounded domain Ω with a boundary $\partial\Omega$ can be written as below:

$$\frac{\partial}{\partial t}\iiint_{\Omega} \boldsymbol{Q}\,\mathrm{d}V + \iint_{\partial\Omega} \boldsymbol{F}(\boldsymbol{Q})\cdot\boldsymbol{n}\,\mathrm{d}S = 0 \tag{1}$$

where $\boldsymbol{Q} = [\rho, \rho\boldsymbol{u}, \rho\boldsymbol{v}, \rho\boldsymbol{w}, \boldsymbol{e}_0]^T$; $\boldsymbol{F}(\boldsymbol{Q})$ is the inviscid flux vector; and variables ρ, $\boldsymbol{u}$, $\boldsymbol{v}$, $\boldsymbol{w}$, and $\boldsymbol{e}_0$ are the density, components of velocity, and total energy per unit volume, respectively.

B. Time Stepping

A dual-time-stepping approach [11] is adopted to advance the time-accuracy solution in time as follows:

$$\frac{\mathrm{d}}{\mathrm{d}\tau}(\boldsymbol{Q}_i^{n+1}V_i^{n+1}) + \boldsymbol{R}^*(\boldsymbol{Q}_i^{n+1}) = 0 \tag{2}$$

$$\boldsymbol{R}^*(\boldsymbol{Q}_i^{n+1}) = \frac{3\boldsymbol{Q}_i^{n+1}V_i^{n+1} - 4\boldsymbol{Q}_i^{n}V_i^{n} + \boldsymbol{Q}_i^{n-1}V_i^{n-1}}{2\Delta t} + \boldsymbol{R}(\boldsymbol{Q}_i^{n+1}) \tag{3}$$

where τ is the pseudotime, V_i^n is the volume of grid element, and $R^*(Q_i^{n+1})$ is the residual. In the simulation of rotor flow, one revolution is divided into 120 time steps. An explicit multistage time-stepping scheme is used to discretize the time derivative in Eq. (2). The solution is advanced from time t to $t + \Delta t$ with a four-stage Runge–Kutta scheme [12], given by

$$\mathbf{W}^{(0)} = (\mathbf{W}^*)_t \qquad \mathbf{W}^{(i)} = \mathbf{W}^{(0)} - \alpha_i\Delta\tau\mathbf{R}^*(\mathbf{W}^{(i-1)})$$
$$(\mathbf{W}^*)_{t+\Delta t} = \mathbf{W}^{(4)} \tag{4}$$

where $i = 1, 2, 3, 4$ is the stage counter for the four-stage scheme and α_i is the multistage coefficient for the ith stage, and they are $\frac{1}{4}$, $\frac{1}{3}$, $\frac{1}{2}$, and 1, respectively, in this Note.

IV. Results and Discussions

A. Simulation of Coaxial Rotor in Hover

The validation of the present method for predicting the unsteady flow around coaxial rotor helicopter was made for the coaxial rotor

Received 26 April 2010; revision received 6 July 2010; accepted for publication 9 July 2010.

*Postdoctoral Researcher, National Key Laboratory of Science and Technology on Aerodynamic Design and Research; xhy2005@mail.nwpu.edu.cn.

†Professor, National Key Laboratory of Science and Technology on Aerodynamic Design and Research; yezy@nwpu.edu.cn.

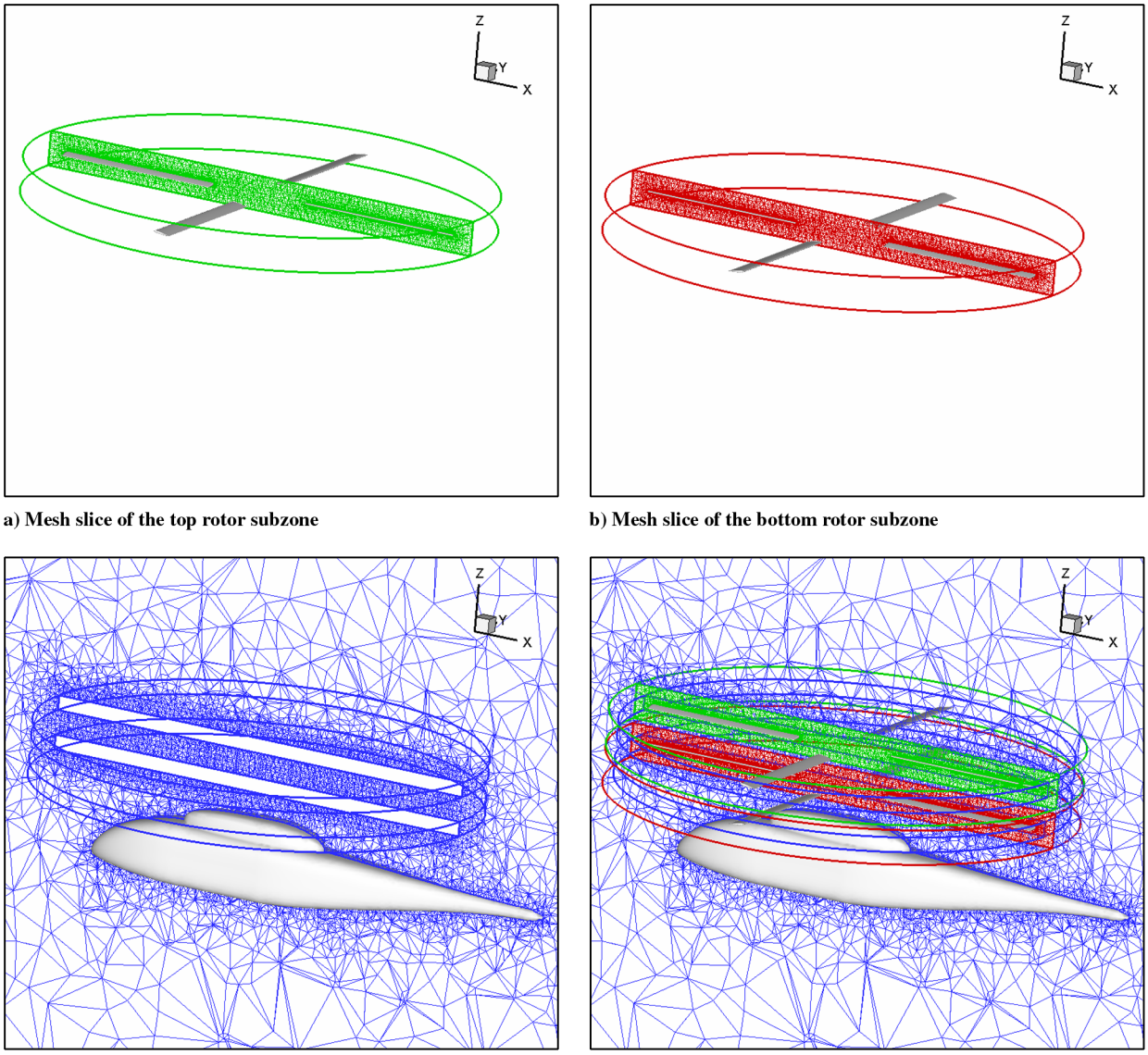

a) Mesh slice of the top rotor subzone

b) Mesh slice of the bottom rotor subzone

c) Mesh slice of the fuselage subzone

d) Mesh slice of all subzones overlapped

Fig. 1 Overlapping mesh of the coaxial-rotor helicopter.

model in hover, which was experimented with in Japan in the late seventh decade of the last century [13]. The hover state is considered as a special forward flight: namely, the advancing ratio is zero. The blades have a NACA0012 airfoil section with no twist angle, and the calculation model has no fuselage. The parameters of coaxial rotor are shown in Table 1.

The slice mesh of the unstructured overset grids is shown in Fig. 2. After a series of unsteady calculations, the variation of thrust coefficient C_T to torque coefficient C_Q is shown in Fig. 3, and they had a fairly good agreement with the experimental data, which demonstrates that the present method is effective and accurate for the prediction of unsteady flow around coaxial rotor.

Table 1 Parameters of experimental coaxial rotors

Name of parameter	Symbol	Value
Radius of rotor	R	0.380 m
Rotor spacing	H	0.260 R
Airfoil chord	c	0.060 m
Root cutout	r_{cut}	21%
Rotational speed	Ω	324.5 rad $\cdot$ s^{-1}
Collective angle	θ	3–12°

From Fig. 3, we can find that the thrust of top rotor is larger than that of the bottom rotor for the same torque coefficient, due to the aerodynamic interaction between the two rotors. For the bottom rotor, the wake vortex of the top rotor directly traverses through the bottom rotor plane into its wake vortex, and the downwash is the collective effect of the two rotors, which results in decreasing the effective attack angle of the bottom rotor. So the thrust of the bottom rotor is smaller than that of the top rotor.

B. Simulation of Coaxial-Rotor Helicopter

The unsteady flow around coaxial rotor helicopter in hover was simulated to investigate the aerodynamic interaction among the two rotors and fuselage. The ROBIN fuselage has an analytical configuration, and the coordinates of the ROBIN body are defined by superellipse equations. The details of the superellipse equations are provided in [14]. The rotor blades are made of NACA0012 airfoil section and have a rectangular planform shape with an aspect ratio of 12.98. The root cutout is at 24% of the radius. The blades have no linear twist and the forward tilt angle of the rotor shaft is 0 deg. The parameters of calculation are shown in detail in Table 2. For the comparison between coaxial rotor helicopter and individual-rotor helicopter, unsteady flow around an individual-rotor helicopter was also simulated, and the configuration of the individual-rotor

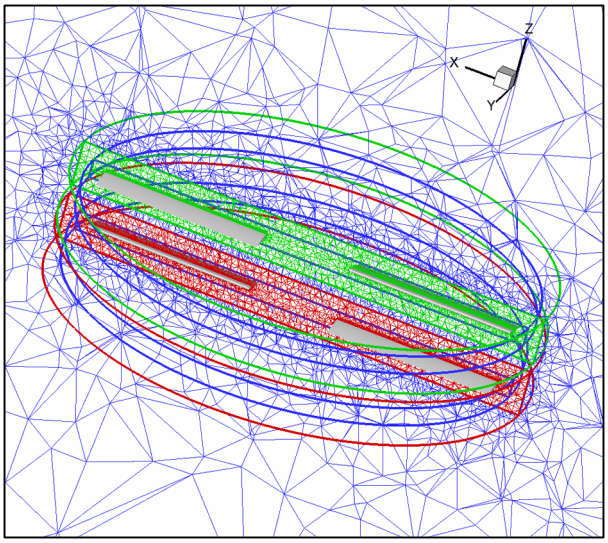

Fig. 2 Overlapping mesh of the coaxial rotors.

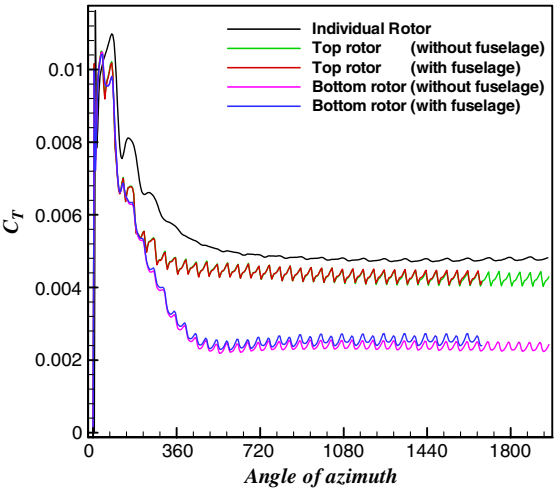

Fig. 4 Comparison of thrust coefficient curves.

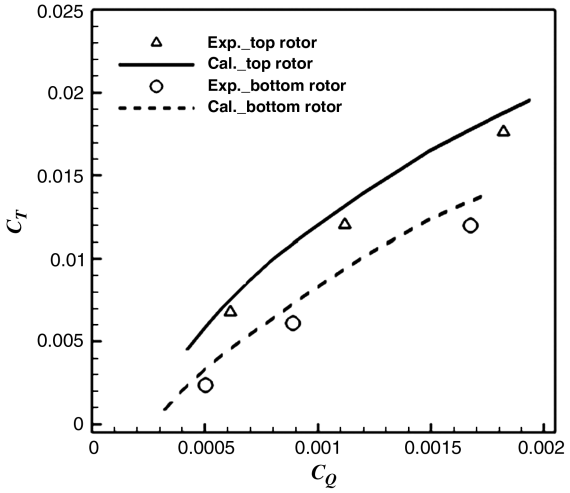

Fig. 3 Comparison of the $C_Q - C_T$ curves.

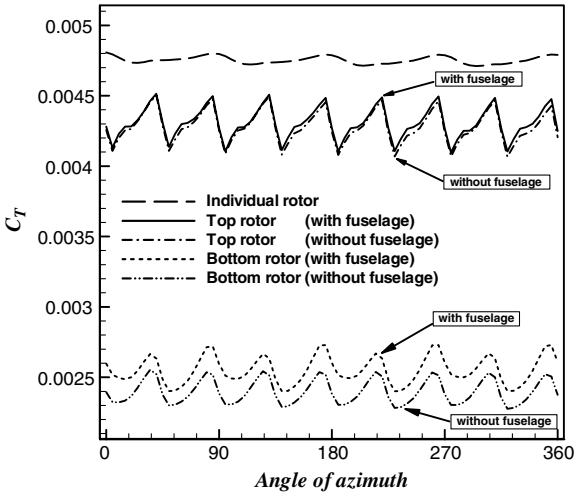

Fig. 5 Magnified comparison of C_T for the last cycle.

helicopter is the coaxial rotor helicopter configuration with the top rotor removed. Additionally, the coaxial rotor system without fuselage was simulated at the same condition, in order to study the effect of fuselage on the rotor.

The thrust coefficients of coaxial rotors with and without fuselage and individual rotor varying with azimuth angle are given in Figs. 4 and 5, and the time-average values of the thrust coefficients $C_{T,\text{average}}$ and fluctuation amplitude δC_T of every rotor are shown in Table 3. For the coaxial rotors with and without fuselage, the thrusts of top rotors are both larger than those of bottom rotors, while the thrust of individual rotor is larger than those of the top rotors. The fluctuation amplitudes of the coaxial rotor thrusts are larger than those of the individual rotor, while the fluctuation amplitudes of the top rotors are a little larger than those of bottom rotors.

The larger fluctuation amplitude of the coaxial rotor thrust compared to the individual rotor demonstrates that the aerodynamic interaction between the two coaxial rotors is much stronger than that between the rotor and fuselage. For the case without fuselage, the average value $C_{T,\text{average}}$ and fluctuation amplitude δC_T of the bottom rotor thrust are both smaller than those of the top rotor, which can be seen from Fig. 5 and Table 3. This can be explained as noted below. The bottom rotor is located in the downwash-induced flow of the top rotor, so the interaction of the top rotor on the bottom rotor is stronger than the effect of the bottom rotor on the top rotor, which leads to a smaller $C_{T,\text{average}}$ and fluctuation amplitude δC_T for the bottom rotor.

For the individual-rotor helicopter model, only the fuselage has aerodynamic interactional influence on the rotor, so the appearance of the fluctuation of thrust is absolutely attributed to the aerodynamic interaction between the rotating rotor and the fuselage when the blades pass through the above region of the fuselage. For the coaxial rotor without fuselage, the two coaxial rotors have strong aerodynamic interactional influence on each other, so the eight locations of the spikes are the encounter locations of the two coaxial rotors, and both the C_T curves present to be equal amplitude. For the coaxial rotor with fuselage, not only the two coaxial rotors have strong aerodynamic interactional influence on each other, but also the fuselage has influence on the rotors, so the spike values of the bottom rotor C_T curve is remarkably nonidentical, due to the influence of the fuselage. The effect of the fuselage on the coaxial rotors can be analyzed from the comparison of the rotor C_T curves with and without fuselage shown in Table 3. The average value $C_{T,\text{average}}$ and

Table 2 Parameters of coaxial-rotor helicopter

Name of parameter	Symbol	Value
Radius of rotor	R	0.86 m
Rotor spacing	H	0.186 R
Tip Mach number	M_{tip}	0.52
Collective angle	θ	8°

Table 3 Comparison of the rotor C_T

	$C_{T,\text{average}}$	δC_T (amplitude of C_T curve)
Individual rotor	4.75×10^{-3}	0.80×10^{-4}
Top rotor (with fuselage)	4.30×10^{-3}	3.88×10^{-4}
Top rotor (without fuselage)	4.27×10^{-3}	3.85×10^{-4}
Bottom rotor (with fuselage)	2.56×10^{-3}	3.28×10^{-4}
Bottom rotor (without fuselage)	2.42×10^{-3}	2.53×10^{-4}

fluctuation amplitude δC_T of coaxial rotors with fuselage are both larger than those without fuselage, and it demonstrates that the existence of fuselage leads to a higher thrust and a larger fluctuation amplitude. Additionally, the discrepancy of $C_{T,\text{average}}$ between the bottom rotors with fuselage and without fuselage is much larger than that between the top rotors, and it demonstrates that the interaction between fuselage and bottom rotor is much stronger than that between fuselage and top rotor, which is obviously because the bottom rotor has a closer distance from the fuselage.

The comparison of downwash velocity at the rotor planes on the longitudinal and lateral sectional planes, respectively, through the center of the rotor disk is given in Fig. 6. The downwash velocity of the top rotor is a little larger than that of the individual rotor, and the downwash velocity of the bottom rotor is much larger than that of the top rotor. This can be explained as noted below. The bottom rotor is located in the outflow of the top rotor, and the top rotor generates a large downwash velocity at the location of the bottom rotor, together with the downwash of the bottom rotor itself, so the resulting collective downwash velocity at the location of the bottom rotor plane is much larger than that of the individual rotor. On the other hand, the discrepancy of the downwash velocity can explain the difference of the thrust values between the coaxial rotors in Fig. 4. Larger downwash velocity decreases the effective attack angle of the bottom rotor, resulting in a smaller thrust coefficient.

The spatial streamlines through the longitudinal midplane at the zero-azimuth-angle blade location are shown in Fig. 7 for both the coaxial and individual-rotor helicopter models, and the shading denotes the different values of downwash velocity. It is found that the flow around the coaxial-rotor helicopter has a stronger downwash than the individual-rotor helicopter, due to the larger thrust generated by the coaxial rotors.

The surface streamlines on the fuselages of coaxial-rotor helicopter and individual-rotor helicopter are both shown in Fig. 8, and the shading denotes the value of downwash velocity. There are upwash vortex flows on the top of the fuselages, and the directions of the vortex are the same as the rotational directions of the bottom rotor and individual rotor, respectively. It is found that the strength of the

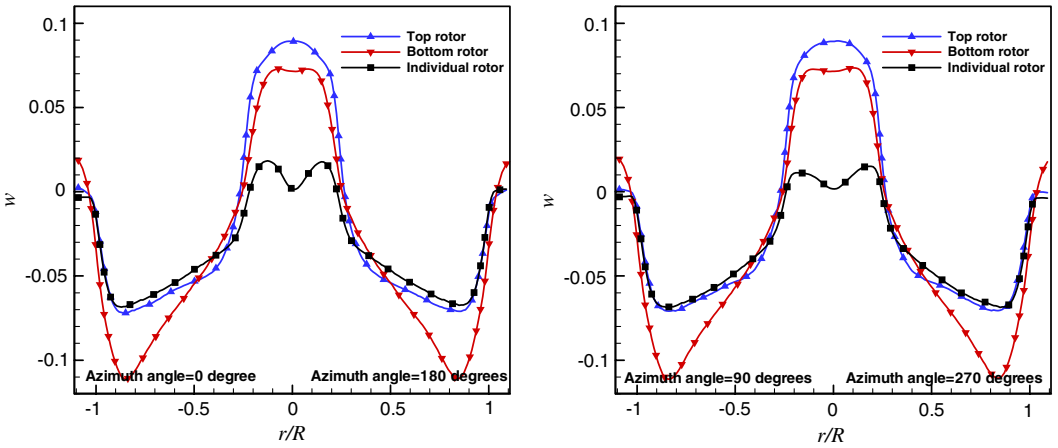

a) Longitudinal **b) Lateral**

Fig. 6 Comparison of the downwash velocity.

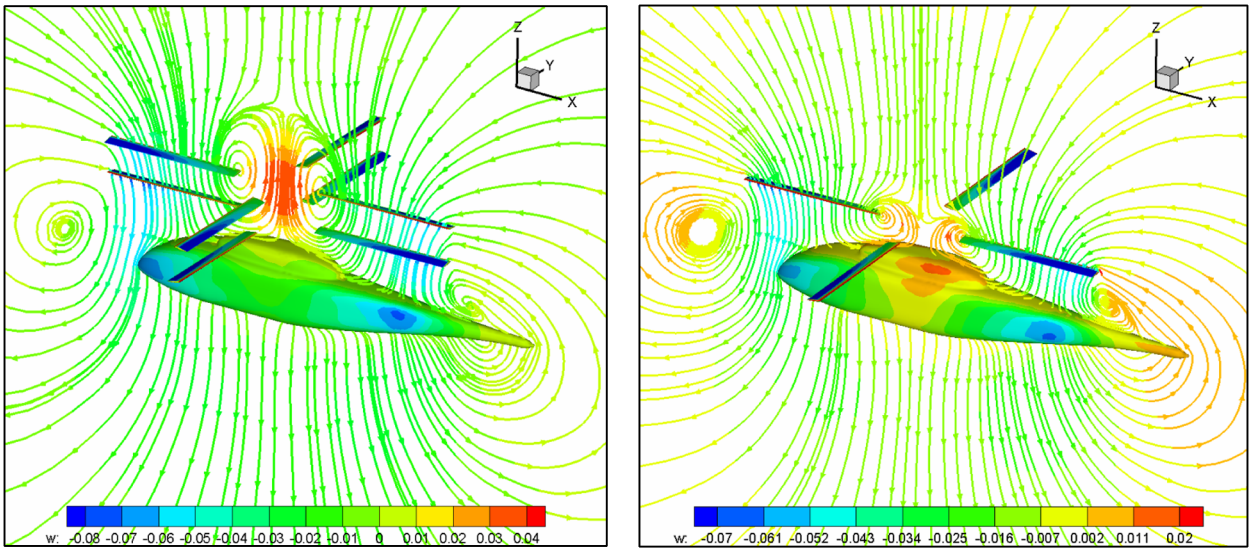

a) Coaxial rotor helicopter **b) Individual rotor helicopter**

Fig. 7 Streamlines on the longitudinal midplane.

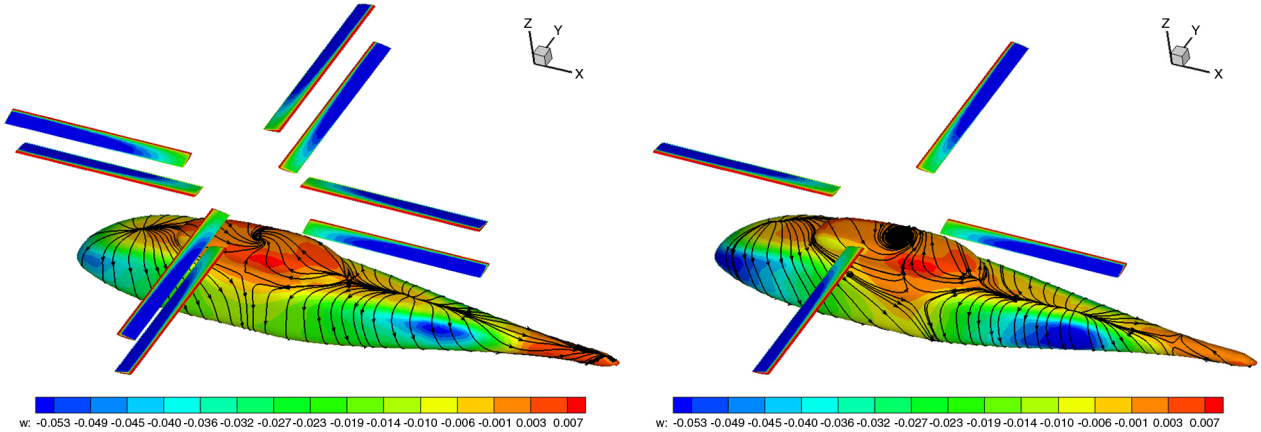

a) Coaxial rotor helicopter **b) Individual rotor helicopter**

Fig. 8 Surface streamlines on the fuselage.

vortex of the coaxial-rotor helicopter model is weaker than that of the individual-rotor helicopter model, because that the converse wake vortex induced by the top rotor decrease the strength of the vortex on the top of the fuselage.

V. Conclusions

In the present Note, both the coaxial-rotor helicopter and the individual-rotor helicopter in hover have been simulated by solving the three-dimensional unsteady Euler equations based on the unstructured dynamic overset grids, and some conclusions are obtained as below.

1) Compared to the individual-rotor helicopter, the thrusts of the two coaxial rotors are both smaller; specifically, the thrust of the bottom rotor is much smaller, which demonstrate that the interaction between the coaxial rotors leads to decreasing the performance of the coaxial rotors, especially for the bottom rotor.

2) The interaction between the coaxial rotors makes the downwash velocity at the bottom rotor plane much larger than that at the individual-rotor plane, and the downwash velocity at the top rotor plane is a little larger than that at the individual-rotor plane.

3) The existence of the fuselage leads to a higher average value and a larger fluctuation amplitude of the rotor thrust.

4) There are upwash vortex flows on the top of the fuselages of both helicopter models, and the strength of the coaxial-rotor helicopter is weaker than that of the individual-rotor helicopter.

Acknowledgments

This work was supported by Chinese Postdoctoral Science Foundation and National Key Laboratory of Science and Technology Foundation of China (9140C42010210ZS51).

References

[1] Andrew, M. J., "Co-Axial Rotor Aerodynamics in Hover," *Vertica*, Vol. 5, 1981, pp. 163–172.

[2] Saito, S., and Azuma, A., "A Numerical Approach to Co-Axial Rotor Aerodynamics," *Vertica*, Vol. 6, 1982, pp. 253–266.

[3] Bagai, A., and Leishman, J. G., "Free-Wake Analysis of Tandem, Tilt-Rotor and Co-Axial Rotor Configurations," *Journal of the American Helicopter Society*, Vol. 41, No. 3, 1996, pp. 196–207. doi:10.4050/JAHS.41.196

[4] Kim, H. W., and Brown, R. E., "A Rational Approach to Comparing the Performance of Coaxial and Conventional Rotors," *Journal of the American Helicopter Society*, Vol. 55, 2010, 012003. doi:10.4050/JAHS.55.012003

[5] Kim, H. W., and Brown, R. E., "A Comparison of Coaxial and Conventional Rotor Performance," *Journal of the American Helicopter Society*, Vol. 55, 2010, 012004. doi:10.4050/JAHS.55.012004

[6] Lakshminarayan, V. K., and Baeder, J. D., "High Resolution Computational Investigation of Trimmed Coaxial Rotor Aerodynamics in Hover," *Journal of the American Helicopter Society*, Vol. 54, No. 4, 2009, Paper 042008. doi:10.4050/JAHS.54.042008

[7] Lakshminarayan, V. K., and Baeder, J. D., "Computational Investigation of Micro-Scale Coaxial Rotor Aerodynamics in Hover," *Journal of Aircraft*, Vol. 47, No. 3, 2010, pp. 940–955. doi:10.2514/1.46530

[8] Lakshminarayan, V. K., and Baeder, J. D., "Computational Investigation of Small Scale Coaxial Rotor Aerodynamics in Hover," AIAA Paper 2009-1069, 2009.

[9] Xu, H. Y., Ye, Z. Y., Wang, G., and Shi, A. M., "Simulation of Helicopter Forward Flight Flow Using Unstructured Overset Grids," AIAA Paper 2009-1285, 2009.

[10] Gleize, V., and Pape, A. L., "Low Mach Number Preconditioning for Unsteady Flow in General ALE Formulation," AIAA Paper 2006-687, 2006.

[11] Jameson, A., "Time Dependent Calculations Using Multi-Grid, with Applications to Unsteady Flows past Airfoils and Wings," AIAA Paper 91-1596, 1991.

[12] Jameson, A., Schmidt, W., and Turkel, E., "Numerical Solutions of the Euler Equations by Finite Volume Methods Using Runge–Kutta Time Stepping Scheme," AIAA Paper 81-1259, 1981.

[13] Colin, P. C., "A Survey of Theoretical and Experimental Coaxial Rotor Aerodynamic Research," NASA TP 3675, 1997.

[14] Raymond, E. M., and Gorton, S. A., "Steady and Periodic Pressure Measurements on a Generic Helicopter Fuselage Model in the Presence of a Rotor," NASA TM 2000-210286, 2000.